

Compressive sensing spectroscopy with a single pixel camera

DAVID J. STARLING,^{1,*} IAN STORER,¹ AND GREGORY A. HOWLAND²

¹Penn State University, Division of Science, 76 University Dr., Hazleton, Pennsylvania 18229, USA

²Air Force Research Laboratory, 525 Brooks Rd., Rome, New York 13441, USA

*Corresponding author: starling@psu.edu

Received 6 April 2016; revised 31 May 2016; accepted 2 June 2016; posted 3 June 2016 (Doc. ID 262586); published 27 June 2016

Spectrometry requires high spectral resolution and high photometric precision while also balancing cost and complexity. We address these requirements by employing a compressive-sensing camera capable of improving signal acquisition speed and sensitivity in limited signal scenarios. In particular, we implement a fast single pixel spectrophotometer with no moving parts and measure absorption and emission spectra comparable with commercial products. Our method utilizes Hadamard matrices to sample the spectra and then minimizes the total variation of the signal. The experimental setup includes standard optics and a grating, a low-cost digital micromirror device, and an intensity detector. The resulting spectrometer produces a 512 pixel spectrum with low mean-squared error and up to a 90% reduction in data acquisition time when compared with a standard spectrophotometer. © 2016 Optical Society of America

OCIS codes: (300.0300) Spectroscopy; (040.0040) Detectors; (050.0050) Diffraction and gratings.

<http://dx.doi.org/10.1364/AO.55.005198>

1. INTRODUCTION

All spectrometers utilize the dispersive properties of a grating or prism to spatially separate the frequency components of a light source. Indeed, a great deal of effort has been placed upon improving optical designs to produce the most accurate spectral images with minimal loss and distortion [1]. However, how this spatial distribution of frequencies is measured differs from one application to the next (e.g., scanning slit versus detector array). Here, we propose and evaluate an alternative design that takes advantage of the benefits of common spectrometers. Namely, we focus on the acquisition of the spatially distributed spectrum by applying methods from compressive sensing (CS) [2,3] to the ubiquitous spectrometer.

A spectrophotometer packages together a light source, a test sample, and a spectrometer to measure the absorption of a material at different wavelengths. The spectrophotometer comes in a variety of designs that vary the dispersive element, the imaging optics, the sample location, and the measurement technique. Additionally, some spectrophotometers have a single beam design [4], where the spectrum is taken with the sample removed and then inserted to calculate absorption; others utilize a two beam design, allowing the reference spectrum to be taken alongside the sample [5]. For either design, one of the primary drivers of cost relies on how the spectrum is measured. These fall into two categories: scanning (e.g., the Cole-Parmer UX-83057-35) and array (e.g., the Ocean Optics USB4000). Most scanning spectrophotometers

(sometimes called monochrometers) employ a mechanically driven slit to scan across the image of the spectrum. For double beam designs, two slits and two detectors are required, both of which must be calibrated before each use. Alternatively, some spectrophotometers use a detector array or CCD, where each pixel corresponds to a range of frequencies. In this configuration, the whole spectrum can be taken quickly (relative to scanning devices) and be displayed in real-time. However, low noise detector arrays inflate the cost of spectrophotometers. For this reason, many high-resolution, high-precision spectrophotometers rely on a scanning slit with a single low-noise detector. In this work, we introduce the use of a 1D CS single-pixel camera [6] to speed up acquisition time while still requiring only a single detector.

Recently, CS has been used to acquire signals at a rate far below the Nyquist frequency by taking advantage of the sparsity of the signal in some known basis [3]. For example, CS is effective for many 2D images [6–8], which tend to be sparse in the wavelet basis. CS also has been used in a variety of other contexts, including hyperspectral imaging [9,10], characterization of high-dimensional single photons [11–13], and microscopy [14–16]. Further work was conducted to improve these results by applying various denoising algorithms in tandem with CS [17].

In the context of spectroscopy, previous work has shown that 2D images can be acquired with both spatial information as well as frequency information [9,10]. These so-called

“hyperspectral” methods combine a dispersive element with CS to construct color images with a monochromatic sensor. However, the frequency resolution of such devices is insufficient for typical spectroscopic measurements. Some recent work has been done in the area of nonlinear spectroscopy using a digital micromirror device (DMD) and CS to map multidimensional electronic structure and ultrafast dynamics [18]. Other work has been done to utilize a DMD for spectroscopic measurements [19]; however, CS was not employed. Additionally, Xu *et al.* presented preliminary work on an Eschelle spectrometer, which utilizes CS and a spatial light modulator to reconstruct spectra from various lamps [20]. The authors produce a number of 2D contour plots of reconstructed images in experiments but do not reduce these results to plots of the spectra. The authors perform a number of simulations and suggest that their technique will be useful for gas tracing.

In what follows, we apply the methods from compressive sensing and Hadamard sensing [21–25] to create a single-pixel spectrometer capable of measuring emission spectra and a spectrophotometer capable of measuring absorption spectra in a single-beam design with a limited signal. We calibrate both designs using mercury lamp emission and a calibrated narrow-band filter. We test the calibrated spectrophotometer with a set of dielectric filters. Results were independently verified using commercial equipment and manufacturer specifications.

2. COMPRESSIVE SENSING

Compressive sensing is a method used to compress a signal during the sensing process, as opposed to compressing it after full acquisition of the signal. This is accomplished by leveraging prior knowledge about effective strategies for compressing classes of signals. Due to this real-time compression, fewer measurements need to be made, resulting in shorter acquisition times.

To describe this compression technique, we typically consider a time-varying signal $f(t)$ that one wishes to acquire with minimal error. Traditionally, the signal must be sampled at or above the Nyquist rate [26]. However, if the signal can be represented in a sparse basis (e.g., the wavelet basis for 2D images), we can undersample the function $f(t)$ at a much lower rate and still reproduce the signal with high fidelity. For maximum efficiency, the signal must be sampled in an incoherent way to avoid correlations between the arbitrary sampling scheme and the signal we wish to acquire [27]. Therefore, in order to apply the concepts of CS, we must have (a) a signal that is sparse in some basis and (b) an incoherent sampling strategy.

In the context of imaging, a number of techniques have been developed that take advantage of image sparsity. In our case, we wish to measure the 1D spectrum $\mathbf{x}(\omega) \in \mathbb{R}$, where ω is the angular frequency of the light. We bin the spectrum into N discrete frequencies such that a typically scanning slit or CCD array would require N measurements or N pixels, respectively. However, utilizing CS, we wish to make $M < N$ measurements represented by a sensing matrix $\mathbf{A} \in \mathbb{R}^{M \times N}$ to obtain the M length measurement vector $\mathbf{y} \in \mathbb{R}$:

$$\mathbf{y} = \mathbf{A} \cdot \mathbf{x}. \tag{1}$$

Many applications solve this set of underdetermined linear equations [Eq. (1)] by minimizing the l_1 norm of $\Phi\mathbf{x}$ subject

to measurement constraints, where unitary Φ transforms \mathbf{x} to a sparse representation. However, based upon the types of spectra we expect to obtain, we solve for \mathbf{x} directly in the pixel basis by taking advantage of its sparsity in the gradient; this is done via total variation (TV) minimization:

$$\min_{\mathbf{x} \in \mathbb{R}^N} \frac{\mu}{2} \|\mathbf{y} - \mathbf{A} \cdot \mathbf{x}\|_2^2 + \text{TV}(\mathbf{x}), \tag{2}$$

where μ is a constant regularization factor, $\|\star\|_2^2$ takes the ℓ_2 norm, and $\text{TV}(\mathbf{x})$ finds the total variation of \mathbf{x} :

$$\text{TV}(\mathbf{x}) = \sum_i \|D_i \mathbf{x}\|. \tag{3}$$

Here, $D_i \mathbf{x}$ is the discrete gradient vector of \mathbf{x} at position i . The first penalty in Eq. (2) is a least-squares penalty that ensures the recovered signal is consistent with measurement results. The second penalty promotes compressibility in the signal’s gradient. Equation (2) is convex and can be solved in a number of ways. Here, we use the TVL3 augmented Lagrangian and alternating direction solver [28].

Last, we must specify the nature of the sensing matrix. We choose \mathbf{A} to be selected from a Hadamard matrix (each element is ± 1) of order N . In particular, we randomly permute the rows of the Hadamard matrix and then randomly select M columns for use in \mathbf{A} . Using a randomly permuted and sampled Hadamard matrix ensures incoherence with and even sampling of \mathbf{x} and allows for fast reconstructions [13,29]. In the following section, we will discuss how the elements of \mathbf{A} correspond to a measurement in the spectrometer.

3. EXPERIMENT

The experimental setup is shown in Fig. 1. The spectrometer consists of a light source, followed by a narrow slit, a 200 mm focal length collimating lens, a 1 cm iris, a stage to place samples, a 600 groove/mm holographic reflective grating, a 50 mm focal length concave mirror, and a DMD. The DMD is placed on a micrometer (transverse) translation stage in order to sample different parts of the spectrum. The light is then directed to a custom photodiode detector using a pair of lenses.

When absorption data is acquired, a broadband (400–800 nm) light-emitting diode (Thorlabs model MWWHL3) is used as the source. The input power to the spectrometer,

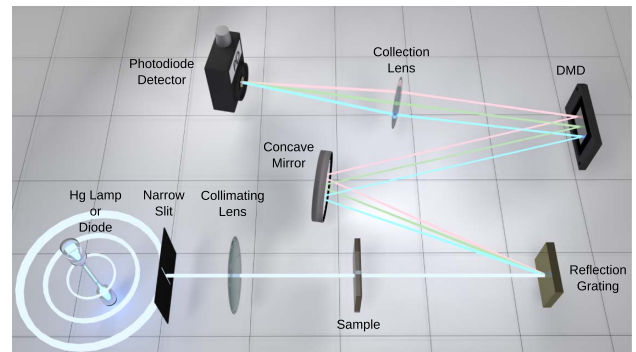


Fig. 1. Experimental setup of the CS spectrometer. The digital micromirror device (DMD) controls which spatial modes are measured by the detector. See text for more details.

measured after the iris, is approximately 100 μW ; however, due to efficiencies in the optical path, only 2.4 μW strike the detector at full illumination. The largest losses come from the DMD, which is not optimized for this particular application, and the diffraction grating, where light is lost to other diffraction orders. In this configuration, test samples are placed after the iris but before the grating. Depending on the application, this placement can be changed as needed.

When emission data are acquired, the source is placed behind the narrow slit, and no sample is used. Otherwise, the setup is unaltered.

In both cases, a Texas Instruments Digital Light Projection LightCrafter Evaluation Module is used with the LED removed. This DMD has a resolution of 608×684 with 10.8 μm pixels and is controlled via computer video output. Because the grating's dispersion (grating vector) is parallel to the plane of the table, the random patterns (one column of the sensing matrix \mathbf{A}) are stretched to form vertical bars, as shown in the inset of Fig. 2. White bars (a 1 in the sensing matrix) indicate that the light at this location is sent to the detector and measured. Black bars (a -1 in the sensing matrix) indicate that light at this location is discarded. Because a -1 implies the light is measured, but contributes a negative value toward the measurement \mathbf{y} , this first measurement is followed by the inverse image, where white and black bars are swapped. (Alternatively, two detectors can be used to measure the power for both ± 1 elements of \mathbf{A} simultaneously, further reducing acquisition time.) The values for \mathbf{y} are the difference in these two measurements. Additionally, we normalize this difference by the total power using the sum of both measurements in order to correct for any drift in the input power. We acquire 511 total measurements for a 512 pixel image (we discard the first column of the Hadamard matrix because it is all 1 s); we then take a subset of these measurements and reconstruct the image from the compressed data.

A 0–6 V signal from the intensity detector is acquired at a rate of 100 kS/s via a 16 bit data acquisition board (model NI

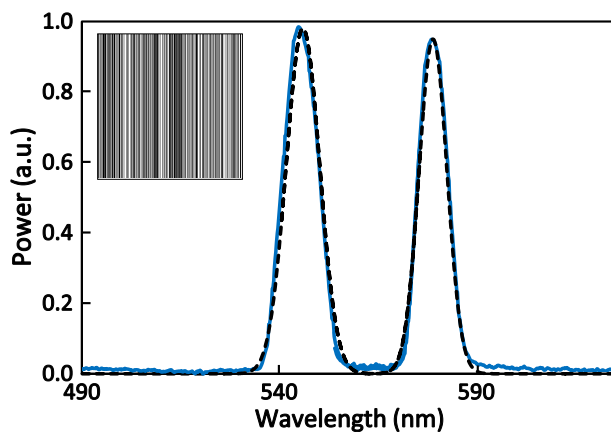


Fig. 2. Calibration of the spectrometer using the 546 and 579 nm lines of a mercury lamp. The emission spectra were reconstructed using CS with 512 measurements at 100 ms each (solid blue curve). We show a best fit of a double Gaussian (dashed black curve) using the Pearson's χ^2 test as the fit parameter. Inset shows a typical DMD pattern constructed from one randomly permuted column of the Hadamard matrix.

USB-6259) controlled by a custom python program. Each measurement integrates for 100 ms and stores the average voltage from the photodiode during the time window. We also measure the voltage offset (dark current) when the DMD is switched off. Data is recorded and then processed (with the offset subtracted) via MATLAB code utilizing TVAL3 [28] with $\mu = 2^4$, $\beta = 2^4$ and a tolerance of e^{-4} .

4. RESULTS

A. Calibration Spectra

We first need to calibrate the spectrometer to determine its resolution and total range. To do so, we use the emission spectrum from a mercury vapor lamp placed before the entrance slit. We measure the 546 and 579 nm lines with the CS spectrometer twice: we translate the DMD 5.1 mm using the micrometer stage to sample the red and blue parts of the spectrum (required for Fig. 3). The results are shown together in Fig. 2 along with a fit line. From this data, we find that the resolution is ~ 0.167 nm/pixel over a range of 86 nm, which agrees well with theoretical calculations based upon the dispersion of the grating and the angles used in the experiment.

Using these results, we tested the absorption of a 10 nm narrowband dielectric filter centered at 570 nm. Using a Gaussian fit and the Pearson's χ^2 test as the fit parameter, we measured the filter to be centered at 567 nm with a FWHM of 10.4 nm, which agrees with the product specifications.

Note that in these measurements we are only using a subset of the DMD (512 of the 608 horizontal pixels) due to technical restrictions of the reconstruction software. However, larger resolution DMDs are available and would provide a proportionally larger range at the cost of acquisition and reconstruction time.

B. Absorption Spectra

Once calibrated (with mercury) and verified (with the 570 nm filter), we chose to consider a variety of absorption wavelengths by testing broadband dielectric filters, as shown in Fig. 3. These curves were created by dividing the spectrum with the filter

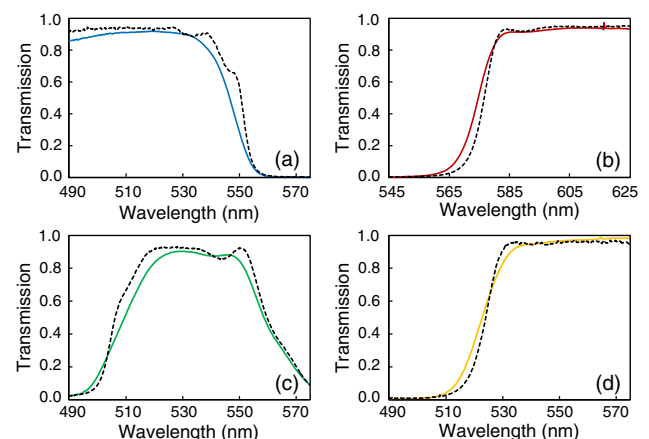


Fig. 3. Measured absorption spectra of four dielectric filters using the CS spectrometer (solid colored curves) and an Ocean Optics spectrometer (dashed black curves). Data were collected for four Thorlabs dichroic filters: (a) blue (FD1B), (b) red (FD1R), (c) green (FD1G), and (d) yellow (FD1Y) using 511 measurements.

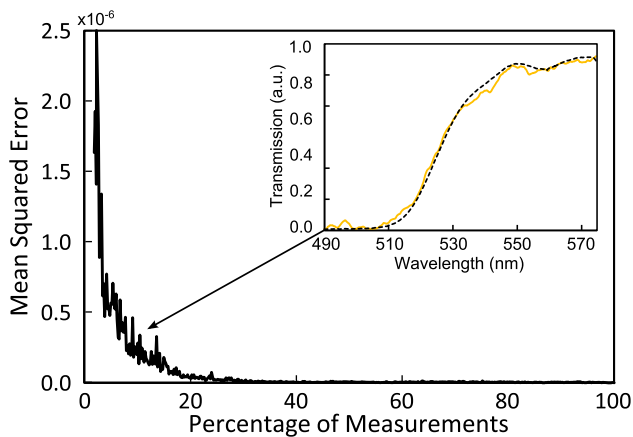


Fig. 4. Mean-squared error in the reconstruction of the yellow absorption spectrum used in Fig. 3(a) for increasing number of measurements M . We only show the data for the yellow filter *in place*. The error is given relative to the reconstructed spectrum using all $M = 511$ measurements. Inset shows the reconstruction for $M = 511$ (dashed black curve) as well as for $M = 53$ (solid yellow curve).

in place by the spectrum with the filter removed. The solid colored lines indicate the CS reconstruction of the spectrum with the calibrated wavelength axis. The dashed black lines are the result from a commercial spectrometer (Ocean Optics USB4000). The results from the CS spectrophotometer match closely to the commercial product.

We should note that these results were obtained using 100 ms integration for each measurement. We also used the full 511 measurements in order to produce the most accurate representation of the spectrum. The reconstruction takes a approximately 100 ms to compute, and the data collection requires 102.2 s of integration per spectrum (51.1 s with the sample in, and 51.1 s with the sample out), which is comparable with commercial single-beam spectrophotometers that utilize a scanning slit. However, the purpose of CS is to reduce the required number of measurements in order to acquire data more rapidly. Therefore, we compared the accuracy of reconstruction of the spectrum for the yellow filter shown in Fig. 3 for increasing M , from as few as 10 measurements up to all 511. We calculate the mean squared error (MSE) between the limited reconstruction and the full reconstruction (with $M = 511$) and show the results in Fig. 4. Note here that we use only a single scan with the sample in place.

From this plot, we see that the MSE drops by 95% from $M = 10$ to $M = 53$ measurements at which point the error slowly decreases toward zero. Therefore, it is possible to obtain an accurate measurement of an 86.0 nm spectrum with a resolution of 0.168 nm/pixel in only 5.3 s. We show the 10% and 100% reconstructed spectra in the inset of Fig. 4.

5. CONCLUSION

We have shown, using a straightforward design, that it is possible to measure absorption or emission spectra with high resolution at a fast rate with very low brightness ($<3 \mu\text{W}$). This design uses CS to reduce the number of measurements by 90% relative to scanning spectrophotometers and results

in spectra that agree well with commercial products. However, it can be seen in Fig. 3 that some detail of the spectra is smoothed out. This is likely a result of chromatic aberration in the first lens, the slit width used, or inadequate control of the image plane of the DMD—and is not due to the reconstruction technique because TV minimization is capable of accurately reproducing piecewise constant signals [30].

Despite these difficulties, we measured a 512-pixel absorption spectrum for five test objects with low error in two wavelength ranges as well as the emission spectrum of a mercury lamp. These spectra can be obtained *with only 53 measurements* (in 5.3 s) and $2.4 \mu\text{W}$ of light. Possible improvements include using a larger DMD with a higher dispersion grating, improving the efficiencies of the various optical elements, and utilizing shot-noise limited detection.

Funding. Air Force Office of Scientific Research (AFOSR) (LRIR 14RI02COR); National Academy of Sciences (NAS) (NRC Associateship); Pennsylvania State University (PSU) (Research Development Grant).

Acknowledgment. Any opinions, findings, and conclusions or recommendations expressed in this material are those of the author(s) and do not necessarily reflect the views of AFRL.

REFERENCES

1. K. W. Kho, P. R. Stoddart, G. Rosman, M. Harris, and A. Mazzolini, "Reduction of polarization-induced artifacts in grating-based spectrometers," *Appl. Opt.* **44**, 6123–6130 (2005).
2. D. L. Donoho, "Compressed sensing," *IEEE Trans. Inf. Theory* **52**, 1289–1306 (2006).
3. E. Candes and M. Wakin, "An introduction to compressive sampling," *IEEE Signal Process. Mag.* **25**, 21–30 (2008).
4. W. Schmidt, "A computerized single-beam spectrophotometer: an easy setup," *Anal. Biochem.* **125**, 162–167 (1982).
5. M. Dubs and H. H. Günthard, "Infrared diode laser double-beam spectrometer," *Appl. Opt.* **17**, 3593–3597 (1978).
6. M. Duarte, M. Davenport, D. Takhar, J. Laska, T. Sun, K. Kelly, and R. Baraniuk, "Single-pixel imaging via compressive sampling," *IEEE Signal Process. Mag.* **25**, 83–91 (2008).
7. M. Duarte and R. Baraniuk, "Kronecker compressive sensing," *IEEE Trans. Image Process.* **21**, 494–504 (2012).
8. Y. Rivenson and A. Stern, "Practical compressive sensing of large images," in *16th International Conference on Digital Signal Processing (IEEE, 2009)*, pp. 1–8.
9. Y. August, C. Vachman, Y. Rivenson, and A. Stern, "Compressive hyperspectral imaging by random separable projections in both the spatial and the spectral domains," *Appl. Opt.* **52**, D46–D54 (2013).
10. T. Sun and K. Kelly, "Compressive sensing hyperspectral imager," in *Frontiers in Optics/Laser Science XXV/Fall*, Optics & Photonics Technical Digest (Optical Society of America, 2009), paper CTuA5.
11. G. A. Howland and J. C. Howell, "Efficient high-dimensional entanglement imaging with a compressive-sensing double-pixel camera," *Phys. Rev. X* **3**, 011013 (2013).
12. F. Tonolini, S. Chan, M. Agnew, A. Lindsay, and J. Leach, "Reconstructing high-dimensional two-photon entangled states via compressive sensing," *Sci. Rep.* **4**, 6542–6547 (2014).
13. D. J. Lum, S. H. Knarr, and J. C. Howell, "Fast Hadamard transforms for compressive sensing of joint systems: measurement of a 3.2 million-dimensional bi-photon probability distribution," *Opt. Express* **23**, 27636–27649 (2015).
14. M. de Moraes Marim, E. D. Angelini, and J.-C. Olivo-Marín, "Compressed sensing in biological microscopy," *Proc. SPIE* **7446**, 744605 (2009).

15. S. Schwartz, A. Wong, and D. A. Clausi, "Compressive fluorescence microscopy using saliency-guided sparse reconstruction ensemble fusion," *Opt. Express* **20**, 17281–17296 (2012).
16. V. Studer, J. Bobin, M. Chahid, H. S. Mousavi, E. Candes, and M. Dahan, "Compressive fluorescence microscopy for biological and hyperspectral imaging," *Proc. Natl. Acad. Sci. USA* **109**, 1679–1687 (2012).
17. C. A. Metzler, A. Maleki, and R. G. Baraniuk, "From denoising to compressed sensing," arXiv: 1406.4175 (2014).
18. A. P. Spencer, B. Spokoyny, S. Ray, F. Sarvari, and E. Harel, "Mapping multidimensional electronic structure and ultrafast dynamics with single-element detection and compressive sensing," *Nat. Commun.* **7**, 10434 (2016).
19. J. D. Batchelor and B. T. Jones, "Development of a digital micromirror spectrometer for analytical atomic spectrometry," *Anal. Chem.* **70**, 4907–4914 (1998).
20. L. Xu, M. A. Davenport, M. A. Turner, T. Sun, and K. F. Kelly, "Compressive echelle spectroscopy," *Proc. SPIE* **8165**, 81650E (2011).
21. E. D. Nelson and M. L. Fredman, "Hadamard spectroscopy," *J. Opt. Soc. Am.* **60**, 1664–1669 (1970).
22. N. J. A. Sloane and M. Harwit, "Masks for Hadamard transform optics, and weighing designs," *Appl. Opt.* **15**, 107–114 (1976).
23. D. K. Graff, "Fourier and Hadamard: transforms in spectroscopy," *J. Chem. Educ.* **72**, 304–309 (1995).
24. L. Streeter, G. R. Burling-Claridge, M. J. Cree, and R. Künnemeyer, "Optical full Hadamard matrix multiplexing and noise effects," *Appl. Opt.* **48**, 2078–2085 (2009).
25. W. Zhang, Z. Zhang, and L. Gao, "Study of using complementary s matrix to enhance {SNR} in Hadamard spectrometer," *Optik* **125**, 1124–1127 (2014).
26. H. Landau, "Sampling, data transmission, and the Nyquist rate," *Proc. IEEE* **55**, 1701–1706 (1967).
27. E. Candes and J. Romberg, "Sparsity and incoherence in compressive sampling," *Inverse Prob.* **23**, 969–985 (2007).
28. C. Li, W. Yin, and Y. Zhang, *User's Guide for TVAL3: TV Minimization by Augmented Lagrangian and Alternating Direction Algorithms* (2010).
29. S. Shishkin, "Fast and robust compressive sensing method using mixed Hadamard sensing matrix," *IEEE J. Emerging Sel. Top. Circuits Syst.* **2**, 353–361 (2012).
30. H. Yu and G. Wang, "Compressed sensing based interior tomography," *Phys. Med. Biol.* **54**, 2791–2805 (2009).